Chinese Journal of Physics 99 (2026) 573–587

Contents lists available at ScienceDirect

Chinese Journal of Physics

journal homepage: www.sciencedirect.com/journal/chinese-journal-of-physics

Research Paper

Activation cross sections of alpha-particle-induced reactions on niobium-93 up to 50 MeV

He Huang [a,*], Masayuki Aikawa [a,b,c], Shuichiro Ebata [d], Kenta Sugihara [e,f,g], Zolbadral Tsoodol [h], Naoyuki Ukon [i], Hiromitsu Haba [g], Sándor Takács [j], Ferenc Ditrói [j], Zoltán Szűcs [j], Tamás Tornyi [j]

[a] Graduate School of Biomedical Science and Engineering, Hokkaido University, Sapporo 060-8638, Japan
[b] Faculty of Science, Hokkaido University, Sapporo 060-0810, Japan
[c] Global Center for Biomedical Science and Engineering, Faculty of Medicine, Hokkaido University, Sapporo 060-8648, Japan
[d] Graduate School of Science and Engineering, Saitama University, Saitama 338-8570, Japan
[e] High Energy Accelerator Research Organization (KEK), Oho, Tsukuba, Ibaraki 305-0801, Japan
[f] The Graduate University for Advanced Studies (SOKENDAI), Hayama, Kanagawa 240-0193, Japan
[g] Nishina Center for Accelerator-Based Science, RIKEN, Wako 351-0198, Japan
[h] Nuclear Research Center, National University of Mongolia, Ulaanbaatar 13330, Mongolia
[i] Advanced Clinical Research Center, Fukushima Medical University, Fukushima 960-1295, Japan
[j] HUN-REN Institute for Nuclear Research (ATOMKI), Debrecen 4026, Hungary

A R T I C L E I N F O

Keywords:
Niobium-93
Alpha-particle induced reactions
Technetium radioisotopes
Cross section
Excitation functions

A B S T R A C T

Technetium radioisotopes have garnered interest in medical applications. In this study, niobium-93 foils were irradiated with a 50-MeV alpha-particle beam to determine the production cross sections of technetium radioisotopes including ^{96g,95m,95g,94g,93m,93g}Tc, along with ^{93m}Mo, ^{95m,95g,92m,91m,90}Nb, ^{89g}Zr and ^{88,87g}Y. The stacked-foil activation technique and gamma-ray spectrometry were adopted for this experiment. The results were compared with the theoretical values of TALYS based TENDL-2023 library, and the previously published experimental data. Physical thick target yields (TTY) were deduced based on the measured cross sections.

1. Introduction

The radionuclides ^{96g}Tc and ^{95g}Tc have been proposed as potential alternatives to the widely used medical radioisotope ^{99m}Tc [1], which serves as a gamma-ray emitter in single-photon emission computed tomography (SPECT) for diagnostic imaging. Compared to ^{99m}Tc ($T_{1/2}$ = 6.0 h), the longer half-lives of ^{96g}Tc ($T_{1/2}$ = 4.3 d) and ^{95g}Tc ($T_{1/2}$ = 20.0 h) make them more suitable for extended transportation and prolonged use in remote medical facilities. ^{94m}Tc has also been considered as a positron emitter for positron emission tomography (PET) [2–4].

The technetium radionuclides with mass numbers $A \leq 97$ can be produced via alpha-particle-induced reactions on the target of the monoisotopic element niobium (^{93}Nb 100 %). However, the available experimental data for the ^{93}Nb(α,x) reactions are not fully consistent, and additional reliable measurements are required.

This study investigated the production cross sections of Tc radionuclides (alongside Mo, Nb, Zr, and Y byproducts) generated via

* Corresponding author.
E-mail address: he@nds.sci.hokudai.ac.jp (H. Huang).

https://doi.org/10.1016/j.cjph.2025.11.038
Received 28 September 2025; Received in revised form 9 November 2025; Accepted 30 November 2025
Available online 1 December 2025

the ^{93}Nb(α,x) reactions. The resulting nuclear data help to optimize radionuclide production for practical applications using alpha-particle beams. Our experimental cross sections are compared with the theoretical values of TALYS code based TENDL-2023 library [5] and existing literature data [6–30].

2. Method

The well-established stacked-foil activation technique was employed for this study. We performed an experiment in which a stacked target composed of niobium foils and natural titanium foils was irradiated with a 50-MeV alpha-particle beam using the AVF cyclotron at RIKEN, Japan. The reaction cross sections were determined through off-line gamma-ray spectrometry performed with a high-purity germanium (HPGe) detector (ORTEC GEM30P4-70).

A niobium foil (Purity: 99.9 %, Thickness: 12.7 μm, Size: 50 × 50 mm; The Nilaco Corporation, Japan) served as the primary target material. A natural titanium foil (Purity: 99.5 %, Thickness: 5 μm, Size: 100 × 50 mm; The Nilaco Corporation, Japan) was used as a beam monitor through the ^{nat}Ti(α,x)^{51}Cr reaction. The areal densities of the Nb and Ti foils were 10.1 and 2.36 mg/cm^2, respectively, determined by measuring their lateral length and weight. The foils were cut to 8 × 8 mm to cover a hole size in a target holder. The target holder also served as a Faraday cup to measure the beam current during the irradiation.

The trimmed foils were arranged in a Nb-Nb-Ti-Ti configuration, repeated 14 times to form the stacked target. Recoiled products from the preceding Nb/Ti foils were captured by the subsequent Nb/Ti foils. Therefore, the recoil product losses of the subsequent Nb/Ti foils were considered to be compensated by those from the preceding Nb/Ti foils. For this reason, gamma-ray spectrum measurements were performed only on the subsequent Nb/Ti foils in each arrangement. The configuration of a single set is presented in Table 1.

The stacked target was irradiated with an alpha-particle beam for 30 min. The average beam intensity was 200 nA, which was determined from the integrated charge using the Faraday cup. The incident beam energy was measured as 51.0 ± 0.2 MeV using the time-of-flight method [31]. Energy degradation through the stacked target was calculated using the stopping power data from SRIM [32]. We used the median energy between incoming and outgoing particles at each foil as the effective projectile energy.

After irradiation, the target was disassembled and gamma-ray spectrometry was done by using HPGe detectors. The detector efficiencies were calibrated at various source-to-detector distances using two point-like calibration sources: a ^{152}Eu source (Japan Radioisotope Association) and a mixed radionuclides source (Eckert & Ziegler Isotope Products). The mixed source contained ten radionuclides ($^{57, 60}$Co, ^{85}Sr, ^{88}Y, ^{109}Cd, ^{113}Sn, ^{137}Cs, ^{139}Ce, ^{203}Hg, and ^{241}Am) emitting multiple gamma-rays, covering an energy range between 60 to 1836 keV. Gamma-ray spectrum analysis was performed using the Gamma Studio software (SEIKO EG&G).

For different half-lives of the radioisotopes of interest, five series of gamma-ray spectrum acquisitions were performed for the Nb foils and three for the Ti foils. The source-to-detector distances were optimized in each case to ensure the detector dead time remained below 3.4 %. A summary of experimental parameters is provided in Table 2. The nuclear reactions investigated, along with their associated decay data were retrieved from NuDat 3.0 [33] and Q-Calc [34], were compiled in Table 3.

Cross sections σ were deduced using the following formula:

$$\sigma = \frac{N_\gamma \lambda}{\varepsilon_\gamma \varepsilon_t I_\gamma N_t N_b (1 - e^{-\lambda t_i}) e^{-\lambda t_c} (1 - e^{-\lambda t_m})} \tag{1}$$

where N_γ is the net count of the peak area of the characteristic gamma-ray, λ is the decay constant (s^{-1}), ε_γ is the detector efficiency for the characteristic gamma-ray at a specific source-to-detector distance, ε_t is the dead time correction factor, I_γ is the characteristic gamma-ray emission intensity of the radionuclide, N_t is the surface density of target atoms (cm^{-2}), N_b is the intensity of incident alpha-particle projectiles (s^{-1}), t_i is the irradiation time (s), t_c is the cooling time (s), and t_m is the measurement time (s).

When the characteristic gamma-ray of the radioisotope of interest was interfered with gamma-rays by another radioisotope, the contribution from the interfering radioisotope N_γ^I was calculated using the following equation and subsequently subtracted from the measured count N_γ:

$$N_\gamma^I = N_\Gamma \frac{\varepsilon_\gamma I'_\gamma}{\varepsilon_\Gamma I_\Gamma} \tag{2}$$

where N_Γ is the net count of another accompanying characteristic gamma-ray from the interfering radioisotope. ε_Γ is the detector efficiency for the accompanying gamma-ray. I'_γ and I_Γ are the emission intensities of the interfered and accompanying gamma-rays for the interfering radioisotope, respectively.

When the radioisotope of interest was also produced by the decay of its parent radioisotope, the independent cross sections were

Table 1
The configuration of a single set in the stacked target (total 14 sets).

Number	Foil	Spectrometry measured or not
1	Nb	No
2	Nb	Yes
3	Ti	No
4	Ti	Yes

Table 2
Experiment parameters.

	Target foils			
	Nb	10.1 ± 0.1 mg/cm^2		
	Ti	2.36 ± 0.02 mg/cm^2		
	Beam			
	Energy		51.0 ± 0.2 MeV	
	Average intensity		200 ± 10 nA	
	Irradiation time		30.0 min	
Measurement	Set number	Cooling time	Distance	Dead time
Nb Series 1	All even-numbered foils	1.6–3.0 h	50–100 cm	0.1–2.7 %
Nb Series 2	All even-numbered foils	3.2–7.8 h	50–100 cm	0.0–1.8 %
Nb Series 3	All even-numbered foils	8.2–36.7 h	5–50 cm	0.0–1.1 %
Nb Series 4	All even-numbered foils	211.7–218.1 h	0–10 cm	0.0–3.0 %
Nb Series 5	All even-numbered foils	293.3–310.0 h	0–2.54 cm	0.0–3.4 %
Ti Series 1	All even-numbered foils	20.5–37.7 h	5 cm	0.0–1.0 %
Ti Series 2	All even-numbered foils	238.7–257.7 h	3 cm	0.0–0.8 %
Ti Series 3	Even-numbered foils (2–18)	317.7–331.8 h	2.54 cm	0.3–0.7 %

determined by subtracting the contribution of the parent radioisotope from the cumulative cross sections, using the following equation [35]:

$$\sigma_d = \sigma_d^{(cum)} - b_{IT}\sigma_p \frac{\lambda_p}{(\lambda_d - \lambda_p)} \left[\frac{\lambda_d \lambda_d}{\lambda_p \lambda_p} \frac{(1 - e^{-\lambda_p t_i}) e^{-\lambda_p t_c} (1 - e^{-\lambda_p t_m})}{(1 - e^{-\lambda_d t_i}) e^{-\lambda_d t_c} (1 - e^{-\lambda_d t_m})} - 1 \right] \tag{3}$$

where $\sigma_d^{(cum)}$ is the cumulative cross section of the daughter radioisotope, σ_d is the independent cross section of daughter radioisotope (direct production), σ_p is the cross section of the parent radioisotope, b_{IT} is the branching ratio of the parent radioisotope decaying to the daughter radioisotope, λ_d and λ_p are the decay constant of the daughter and parent radioisotope, respectively.

The cross sections of the ^{nat}Ti(α,x)^{51}Cr monitor reaction were derived using the Eq. (1), and compared with the recommended values provided by IAEA [36,37]. We applied a correction of +0.2 MeV to the beam energy (within its uncertainty range) and adjusted the beam intensity by −3 % to improve agreement with the reference data. The comparison is shown in Fig. 1, presenting both uncorrected and corrected results. The other measured values of the beam parameters and foil thicknesses were directly adopted without any adjustments.

The total uncertainties in the beam energy for each foil were propagated from the uncertainties in the primary beam energy (0.2 MeV) and target thickness (1 %). The total uncertainties in the cross section values included contributions from the target thickness (1 %), foil purity (1 %), beam intensity (5 %), detector efficiency (5 %), gamma-ray intensities (< 3 %), and counting statistics (0.5 - 40.6 %).

The physical thick target yields α_{phys} [38] is estimated from the interpolated excitation function obtained from the experimentally determined cross section data using the following formula:

$$\alpha_{phys} = \lambda \int_0^{E_0} dE \left(-\frac{1}{\rho} \frac{dE}{dx} \right)^{-1} \sigma(E) \Big/ (Ze) \tag{4}$$

Where E_0 is initial beam energy, $-(1/\rho)(dE/dx)$ is the stopping power, Z is the charge number of the projectile, e is the elementary charge.

3. Results and discussion

Production cross sections of ^{96g,95m,95g,94g,93m,93g}Tc, ^{93m}Mo, ^{95m,95g,92m,91m,90}Nb, ^{89g}Zr and ^{88,87g}Y were determined in this experiment. The obtained cross sections were summarized in Table 4 and shown graphically in Figs. 2–16 in comparison with the theoretical values from TALYS code based TENDL-2023 data library [5], as well as the previously reported experimental data [6–30] found in the EXFOR data library [39]. The physical thick target yields [38] for the measured radionuclides were determined based on the interpolation of the measured cross sections, and are illustrated in Figs. 17 and 18.

3.1. Production cross sections of ^{96}Tc

^{96}Tc isotope can be produced via the ^{93}Nb(α,n)^{96}Tc reaction, which has a threshold energy of 7.3 MeV. The ^{96}Tc has a metastable state (^{96m}Tc) and a ground state (^{96g}Tc).

The metastable state, ^{96m}Tc, has a half-life of 51.5 min and decays to the ground state via isomeric transition (IT) with a probability of 98 %. The gamma line at 1200.15 keV (^{96m}Tc: Iγ = 1.1 %) was detected in niobium foils corresponding to beam energies of 13.9 and

Table 3
Possible reactions and decay data of reaction products. Gamma lines in bold were adopted to derive cross sections. The reactions with the highest Q-values are listed for the specified target isotopes and residuals.

Nuclide	E[level] (keV)	Half-life	Decay mode (%)	E_g (keV)	I_g (%)	Contributing Reaction	Q-Value (MeV)	Threshold Energy (MeV)
^{51}Cr	0.0	27.704 d	ε: 100	**320.0824**	**9.91**	^{47}Ti(α,γ)^{51}Cr	8.9	0.0
						^{48}Ti(α,n)^{51}Cr	− 2.7	2.9
						^{49}Ti(α,2n)^{51}Cr	− 10.8	11.6
						^{50}Ti(α,3n)^{51}Cr	− 21.8	23.4
^{96g}Tc	0.0	4.28 d	ε+β$^+$: 100	778.22	99.760	^{93}Nb(α,n)^{96}Tc	− 7.0	7.3
				812.54	**82 (3)**			
				849.86	98 (4)			
				1126.85	15.2 (12)			
^{96m}Tc	34.234	51.5 min	IT: 98.0 (5)	778.22	1.9 (5)			
			ε+β$^+$: 2.0 (5)	**1200.15**	**1.1 (3)**			
^{95g}Tc	0.0	20.0 h	ε+β$^+$: 100	**765.789**	**93.8 (3)**	^{93}Nb(α,2n)^{95}Tc	− 14.9	15.4
				1073.71	3.74 (4)			
^{95m}Tc	38.9	61 d	IT: 3.88 (32)	204.117	63.2 (8)			
			ε+β$^+$: 96.12 (32)	**582.082**	**29.9 (4)**			
				835.149	26.6 (4)			
^{94g}Tc	0.0	293 min	ε+β$^+$: 100	**702.67**	**99.6 (18)**	^{93}Nb(α,3n)^{94}Tc	− 24.8	25.7
				849.74	95.7 (18)			
				871.05	99.9			
^{94m}Tc	76	52.0 min	ε+β$^+$: 100	871.05	94.2 (5)			
				993.19	2.21 (3)			
				1522.1	4.5 (3)			
				1868.68	**5.7 (3)**			
^{93g}Tc	0.0	2.75 h	ε+β$^+$: 100	**1362.94**	**66.2 (6)**	^{93}Nb(α,4n)^{93}Tc	− 33.5	34.7
				1477.14	8.7 (5)			
				1520.28	24.4 (8)			
^{93m}Tc	391.83	43.5 min	IT: 77.4 (6)	**391.83**	**58.3 (9)**			
			ε+β$^+$: 22.6 (6)	2644.6	14.3 (6)			
^{93m}Mo	2424.97	6.85 h	IT: 99.8832 (24)	263.049	57.4 (11)	^{93}Nb(α,n+t)^{93}Mo	− 21.0	21.7
			ε+β$^+$: 0.1169 (24)	**684.693**	**99.9 (8)**			
				1477.138	99.1 (11)			
^{95g}Nb	0.0	34.991 d	β$^-$: 100	**765.803**	**99.808 (7)**	^{93}Nb(α,2p)^{95}Nb	− 12.6	13.0
^{95m}Nb	235.69	3.61 d	β$^-$: 5.6 (6)	**235.69**	**24.8 (8)**			
			IT: 94.4 (6)					
^{92m}Nb	135.5	10.15 d	ε+β$^+$: 100	**934.44**	**99.15 (4)**	^{93}Nb(α,n+p+t)^{92}Nb	− 28.6	29.7
^{91m}Nb	104.6	60.86 d	IT: 96.6 (5)	**1204.67**	**2.02 (8)**	^{93}Nb (α,3n+p+d)^{91}Nb	− 42.8	44.3
^{90g}Nb	0.0	14.60 h	ε+β$^+$: 100	**141.178**	**66.8 (7)**	^{93}Nb(α,3n+α)^{90}Nb	− 28.8	29.8
				1129.224	92.7 (5)			
^{89g}Zr	0.0	78.41 h	ε+β$^+$: 100	**909.15**	**99.04 (3)**	^{93}Nb(α,n+t+α)^{89}Zr	− 25.4	26.3
^{88g}Y	0.0	106.627 d	ε+β$^+$: 100	898.042	93.7 (3)	^{93}Nb(α,n+2α)^{88}Y	− 13.4	13.9
				1836.063	**99.2 (3)**			
^{87g}Y	0.0	79.8 h	ε+β$^+$: 100	388.5276	82.2 (7)	^{93}Nb(α,2n+2α)^{87}Y	− 22.8	23.6
				484.805	**89.8 (9)**			

18.6 MeV, indicating relatively large production of ^{96m}Tc. However, due to significant statistical uncertainties (> 30 %), cross sections for ^{96m}Tc were not quantified in this study.

The ground state ^{96g}Tc has a half-life of 4.3 d, and its cross sections could be determined by counting the gamma line at 812.5 keV ($I\gamma$ = 82 %). The measurement in Ser. 4 was adopted, during which the metastable state had fully decayed. Considering the contribution from its metastable state's IT decay (98.0 %), the results were cumulative and shown in Fig. 2.

Our results were compared with the previously published data [7–10,13–16,18–20,22–25,27–29] found in the EXFOR data library [39] and the theoretical prediction in the TENDL-2023 library [5]. The previously published data have some differences in description. Some reported cumulative cross sections of ^{96g}Tc and others $^{96(g+m)}$Tc. Given that ^{96m}Tc decays almost entirely to ^{96g}Tc within a short period, all reported values were compared with our results in Fig. 2. Our results show good agreement with some of the previously published data and the theoretical values.

3.2. Production cross sections of ^{95}Tc

^{95}Tc can be produced via the ^{93}Nb(α,2n)^{95}Tc reaction, with a threshold energy of 15.4 MeV. ^{95}Tc has a ground state (^{95g}Tc) and a metastable state (^{95m}Tc). The metastable state ^{95m}Tc has a half-life of 61.9 d, which is significantly longer than that of its ground state ^{95g}Tc (19.3 h).

The cross sections of ^{95m}Tc were determined by the photopeak at 204.1 keV after cooling time of 293.4 - 315.5 h. The results are

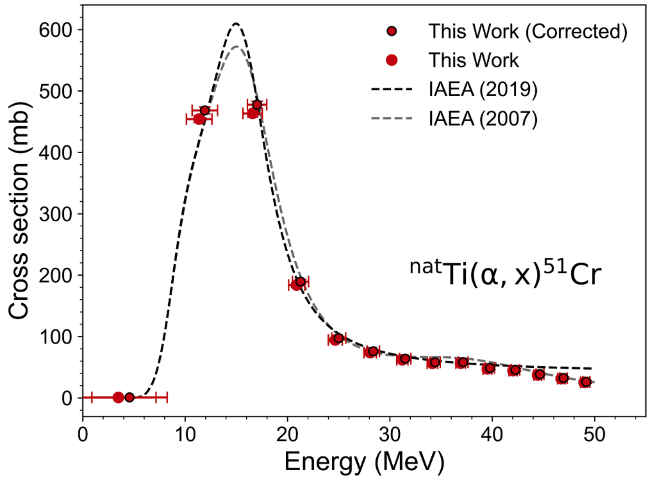

Fig. 1. The cross sections of the $^{nat}Ti(\alpha,x)^{51}Cr$ monitor reaction, compared with the IAEA recommended values [36,37].

Table 4
Cross sections (mb) determined in this work.

Energy (MeV)	$^{93}Nb(\alpha,n)^{96g}Tc$ (cum)	$^{93}Nb(\alpha,2n)^{95m}Tc$	$^{93}Nb(\alpha,2n)^{95g}Tc$	$^{93}Nb(\alpha,3n)^{94g}Tc$	$^{93}Nb(\alpha,4n)^{93m}Tc$	$^{93}Nb(\alpha,4n)^{93g}Tc$ (cum)	$^{93}Nb(\alpha,x)^{93m}Mo$
50.0 ± 0.4	3.56 ± 0.29	4.2 ± 0.4	48 ± 4	352 ± 27	11.7 ± 2.3	366 ± 28	195 ± 15
47.8 ± 0.4	4.07 ± 0.33	4.8 ± 0.5	58 ± 5	459 ± 35	10.7 ± 2.7	299 ± 23	141 ± 11
45.5 ± 0.4	4.7 ± 0.4	5.5 ± 0.5	70 ± 5	590 ± 40		214 ± 17	82 ± 7
43.1 ± 0.4	5.4 ± 0.4	7.4 ± 0.6	85 ± 6	720 ± 50		113 ± 9	35 ± 4
40.7 ± 0.4	6.5 ± 0.5	9.4 ± 0.8	124 ± 9	810 ± 60		41 ± 4	10.0 ± 2.0
38.1 ± 0.5	7.8 ± 0.6	12.3 ± 1.0	195 ± 14	810 ± 60		5.2 ± 1.5	
35.4 ± 0.5	9.8 ± 0.8	21.1 ± 1.6	329 ± 24	720 ± 50			
32.6 ± 0.5	13.1 ± 1.1	37.3 ± 2.8	600 ± 40	470 ± 40			
29.5 ± 0.6	18.6 ± 1.5	71 ± 5	920 ± 70	126 ± 10			
26.3 ± 0.7	32.6 ± 2.6	103 ± 8	1020 ± 70				
22.7 ± 0.7	113 ± 9	106 ± 8	840 ± 60				
18.6 ± 0.9	470 ± 40	50 ± 4	322 ± 23				
13.9 ± 1.1	264 ± 21						
7.7 ± 1.8	0.089 ± 0.008						

Energy (MeV)	$^{93}Nb(\alpha,2p)^{95m}Nb$	$^{93}Nb(\alpha,2p)^{95g}Nb$	$^{93}Nb(\alpha,x)^{92m}Nb$	$^{93}Nb(\alpha,x)^{91m}Nb^{(cum)}$	$^{93}Nb(\alpha,x)^{90(g+m)}Nb$	$^{93}Nb(\alpha,x)^{89g}Zr^{(cum)}$	$^{93}Nb(\alpha,x)^{88(g+m)}Y$	$^{93}Nb(\alpha,x)^{87g}Y^{(cum)}$
50.0 ± 0.4	0.093 ± 0.021	2.79 ± 0.21	25.6 ± 1.9	10.7 ± 2.6	43.6 ± 3.3	0.119 ± 0.019	2.74 ± 0.24	0.129 ± 0.019
47.8 ± 0.4	0.127 ± 0.027	2.52 ± 0.20	23.5 ± 1.7	7.2 ± 2.3	19.2 ± 1.5		1.89 ± 0.20	
45.5 ± 0.4	0.118 ± 0.027	2.67 ± 0.21	22.7 ± 1.6	9.7 ± 2.8	4.9 ± 0.5		1.14 ± 0.15	
43.1 ± 0.4	0.080 ± 0.029	2.47 ± 0.20	20.5 ± 1.5	8.5 ± 2.5			0.56 ± 0.09	
40.7 ± 0.4	0.096 ± 0.029	2.51 ± 0.20	19.1 ± 1.4	9.6 ± 2.8			0.23 ± 0.06	
38.1 ± 0.5		2.38 ± 0.19	17.1 ± 1.2	6.3 ± 2.5				
35.4 ± 0.5			16.0 ± 1.2					
32.6 ± 0.5			15.0 ± 1.1					
29.5 ± 0.6			12.3 ± 0.9					
26.3 ± 0.7			8.0 ± 0.6					
22.7 ± 0.7			2.44 ± 0.19					

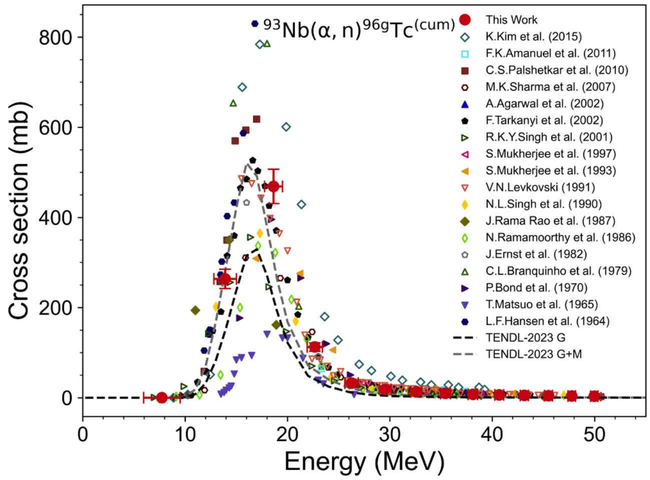

Fig. 2. Cumulative cross sections of the ^{93}Nb(α,n)^{96g}Tc reaction, compared with the previously published data [7–10,13–16,18–20,22–25,27–29] and the theoretical values from the TENDL-2023 library [5].

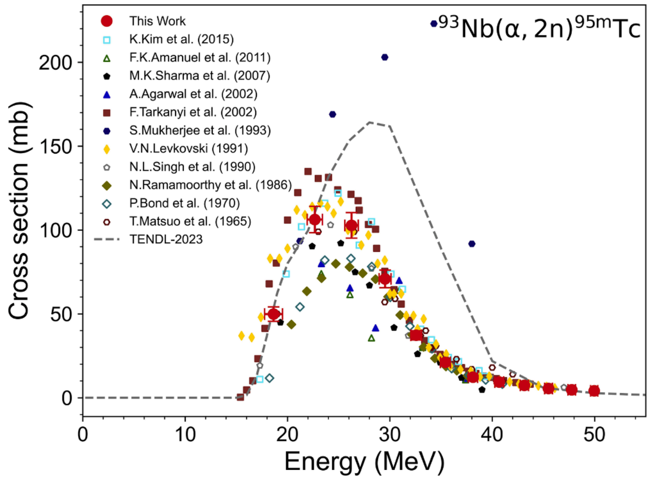

Fig. 3. Cross sections of the ^{93}Nb(α,2n)^{95m}Tc reaction, compared with the previously published data [7,8,10,13,14,18–20,23,27,28] and the theoretical values from the TENDL-2023 library [5].

shown in Fig. 3. The former published studies [7,8,10,13,14,18–20,23,27,28] provided cross sections of ^{95m}Tc. Their results and theoretical prediction in the TENDL-2023 data library [5] were compared with ours.

As for the production cross section of ^{95g}Tc, although the contribution of ^{95m}Tc decay to ^{95g}Tc production during cooling was minimal (IT: 3.88 %), it was initially treated as cumulative values. These cumulative cross sections were derived by analyzing the 765.8-keV gamma line after cooling time ranging from 17.4 to 36.7 h (Ser. 3). Eq. (3) was then applied to correct for the contribution from ^{95m}Tc, and the resulted independent cross sections were less different from the original cumulative values.

Furthermore, ^{95g}Nb, which has a relatively long half-life of 35.0 d and also emits the 765.8-keV gamma line, interferes with the measurement. Its contribution to the total gamma counts in Ser. 3 was estimated based on the results from measurements in Ser. 5 and its decay curve, and was subsequently subtracted. Thus, independent cross sections of ^{95g}Tc are obtained and shown in Fig. 4.

The literature values [7–10,12–16,18–20,22–25,27,28] and the theoretical prediction in the TENDL-2023 data library [5] were consequently compared with our experimental results in Fig. 4. Although the previous works [7,8,10,14,15,18–20,23,24,27,28] did not explicitly state this, their reported values likely correspond to cumulative ^{95g}Tc cross sections. Mukherjee et al. [12] and Branquinho et al. [25] reported total cross sections of $^{95(g+m)}$Tc along with isomeric ratios. From these data, we derived their ^{95g}Tc cross sections for comparison with our measurements. Palshetkar et al. [9], Mukherjee et al. [16] and Rao et al. [22], provided only total cross sections of $^{95(g+m)}$Tc, which are labeled as “G+M” in Fig. 4. Tarkanyi et al. [13] employed short irradiation and cooling periods to minimize the contribution via ^{95m}Tc decay. Consequently, their reported cross sections represent independent production values and are designated “Ind.” in Fig. 4. Our results show good agreement with the most recently published data and are slightly higher than values from TENDL-2023.

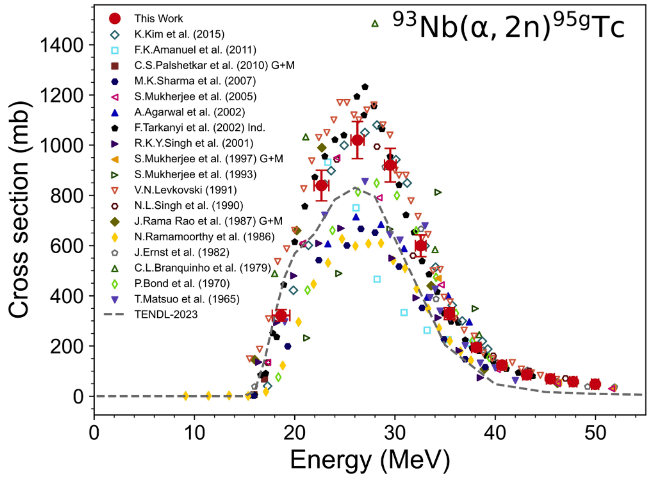

Fig. 4. Cross sections of the ^{93}Nb(α,2n)^{95g}Tc reaction, compared with the previously published data [7–10,12–16,18–20,22–25,27,28] and the theoretical values from the TENDL-2023 library [5].

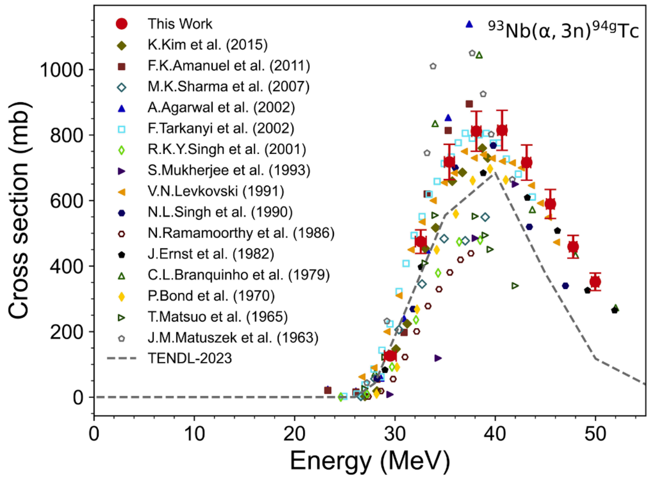

Fig. 5. Cross sections of the ^{93}Nb(α,3n)^{94g}Tc reaction, compared with the previously published data [7,8,10,13–15,18–20,23–25,27,28,30] and the theoretical values from the TENDL-2023 library [5].

3.3. Production cross sections of ^{94}Tc

^{94}Tc can be produced via the ^{93}Nb(α,3n)^{94}Tc reaction, with a threshold energy of 25.7 MeV. ^{94}Tc has a ground state and a metastable state, that are not related through parent-daughter decay. Both states decay exclusively via electron capture and β^+ decay. The cross sections of metastable state ^{94m}Tc ($T_{1/2}$ = 52 min) were not quantified in this work due to large statistical uncertainties exceeding 40 %

The independent cross sections of the ground state ^{94g}Tc ($T_{1/2}$ = 293 min) were measured by analyzing the 702.7-keV gamma line after cooling time ranging from 3.2 to 6.1 h. Our results were compared with those reported in the references [7,8,10,13–15,18–20,23–25,27,28,30] and the theoretical prediction in the TENDL-2023 library [5] in Fig. 5.

Among these literature data, Branquinho et al. [25] provided total cross sections of $^{94(g+m)}$Tc and the isomeric ratios. Based on these data, the cross sections of ^{94g}Tc were calculated and compared with our results in Fig. 5. Our data are consistent with some of the previously published values and are slightly higher than those predicted by TENDL-2023.

3.4. Production cross sections of ^{93}Tc

^{93}Tc can be produced via the ^{93}Nb(α,4n)^{93}Tc reaction, which has a threshold energy of 34.7 MeV. ^{93}Tc has ground and metastable states. The metastable state ^{93m}Tc undergoes the isomeric transition to ^{93g}Tc with a branching ratio of 77.4 %.

The cross sections of ^{93m}Tc were determined by analyzing the 391.8-keV gamma line. The signals were only observed and

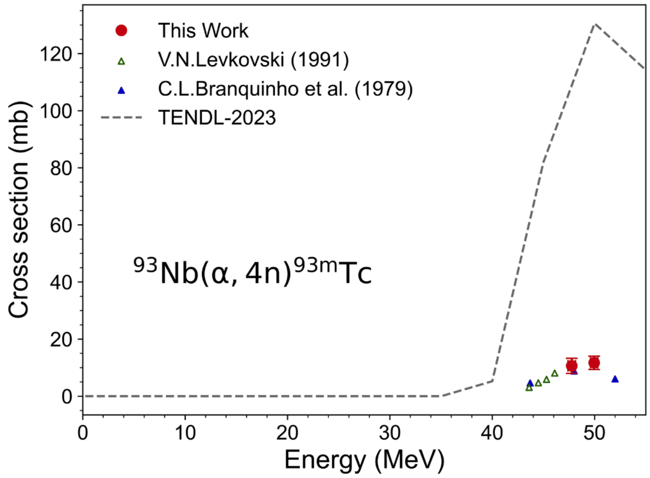

Fig. 6. Cross sections of the ^{93}Nb(α,4n)^{93m}Tc reaction, compared with the previously published data [19,25] and the theoretical values from the TENDL-2023 library [5].

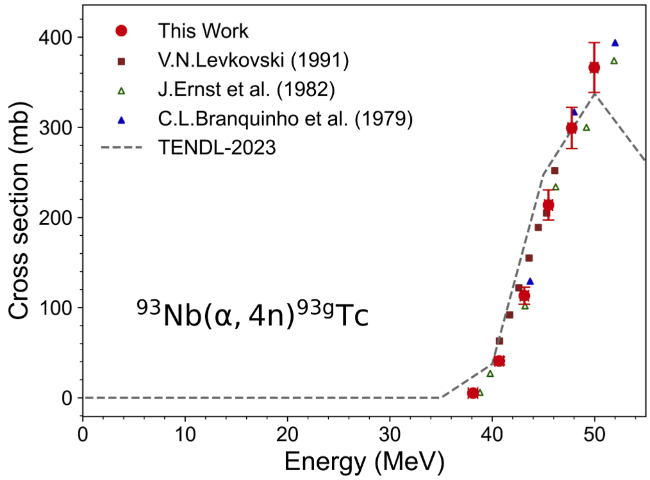

Fig. 7. Cumulative cross sections of the ^{93}Nb(α,4n)^{93g}Tc reaction, compared with the previously published data [19,24,25] and the theoretical values from the TENDL-2023 library [5].

quantified in the two foils at the highest energy. Due to its short half-life (43.4 min), spectra with cooling time of 1.8–1.9 h were used. Our results were compared with those from former studies [19,25] and theoretical prediction in the TENDL-2023 library [5], shown in Fig. 6. The comparison shows that TENDL-2023 overestimates the ^{93m}Tc cross sections.

The cross sections of ^{93g}Tc ($T_{1/2}$ = 2.8 h) are shown in Fig. 7. The cumulative cross sections were determined by analyzing the 1362.9-keV gamma line after 3.2–5.0 h, including minor contributions from ^{93m}Tc. Our results were compared with the previous studies [19,24,25] and the theoretical prediction in the TENDL-2023 library [5] in Fig. 7. The ^{93g}Tc and ^{93m}Tc results reported by Branquinho et al. [25] were derived from their published total cross sections of $^{93(g+m)}$Tc and corresponding isomeric ratios. Our results are in good agreement with the previously published data and the theoretical values from TENDL-2023 at energies below 50 MeV.

3.5. *Production cross sections of ^{93m}Mo*

^{93}Mo can be produced through the ^{93}Nb(α,x)^{93}Mo reaction (E_{th} = 21.7 MeV). The ground state ^{93g}Mo ($T_{1/2} = 4 \times 10^3$ y) does not emit detectable gamma rays. The cross sections of ^{93m}Mo ($T_{1/2}$ = 6.9 h) were determined by analyzing the 684.7-keV gamma line after cooling time of 29.4–36.7 h.

Our results were compared with the previously published data [6,8,18–20,24,25] and the theoretical values from the TENDL-2023 library [5] shown in Fig. 8. The data reported by Branquinho et al. [26] shows larger cross sections, while those by Singh et al. [20] are smaller.

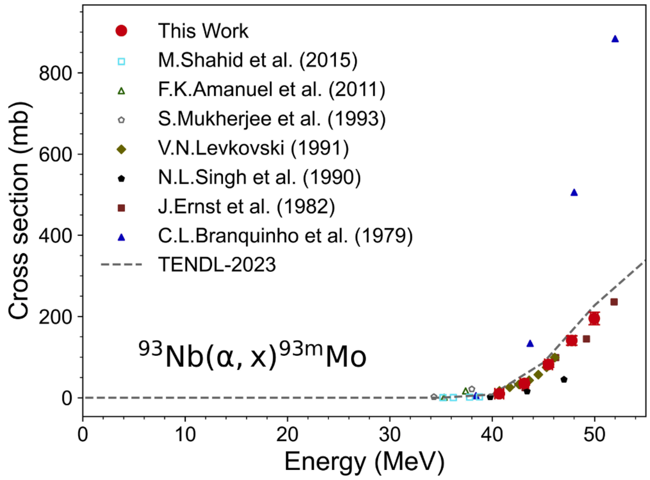

Fig. 8. Cross sections of the ^{93}Nb(α,x)^{93m}Mo reaction, compared with the previously published data [6,8,18–20,24,25] and the theoretical values from the TENDL-2023 library [5].

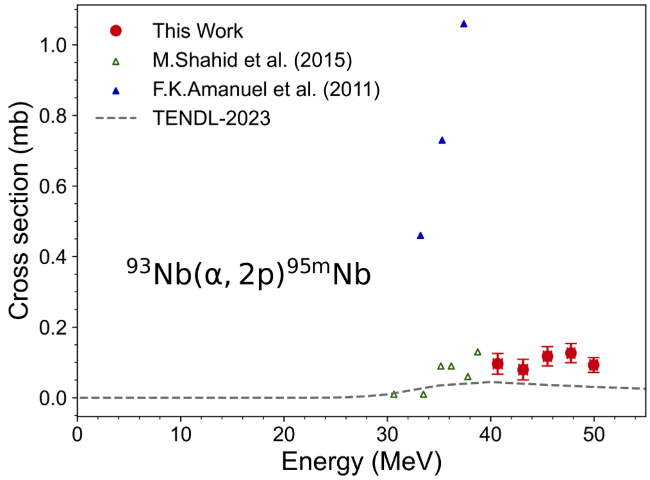

Fig. 9. Cross sections of the ^{93}Nb(α,2p)^{95m}Nb reaction, compared with the previously published data [6,8] and the theoretical values from the TENDL-2023 library [5].

3.6. Production cross sections of ^{95}Nb

^{95}Nb can be produced via the ^{93}Nb(α,2p)^{95}Nb reaction with a threshold energy of 13.0 MeV. The ^{95}Nb has two long-lived energy levels: the metastable state ^{95m}Nb ($T_{1/2}$ = 3.6 d) and the ground state ^{95g}Nb ($T_{1/2}$ = 35.0 d). ^{95m}Nb decays to its ground state through isomeric transition with a branching ratio of 94.4 %.

The cross sections of ^{95m}Nb were determined by analyzing the gamma line at 235.7 keV in spectra measured after cooling time of 211.8–216.0 h. The results were compared with the previously published data [6,8] and the theoretical prediction values in the TENDL-2023 library [5]. The results reported by Amanuel et al. [8] are much larger than the other experimental cross sections.

The cross sections of ^{95g}Nb were initially determined using the gamma line at 765.8 keV, after long cooling time of 311.0–316.5 h. The contributions from the parent isotope ^{95m}Nb were accounted using the equation (3) then and subsequently subtracted.

However, an interference exists from the closely overlapping 765.8-keV gamma-ray (Iγ = 93.8 %) emitted by ^{95g}Tc ($T_{1/2}$ = 20.0 h) in equilibrium with the decay of long-lived ^{95m}Tc ($T_{1/2}$ = 61 d). The contribution from this interference can be evaluated using the Eq. (2), combined with the characteristic gamma-ray of ^{95g}Tc at 1073.7 keV (Iγ = 3.74 %), measured in the same series. The 1073.7-keV gamma line was detected at projectile energies equal to or below 35.4 MeV, but with large uncertainties (>22 %). Due to the potential impact on the cross section data, and the substantial associated uncertainties, the corrected results are presented only for energies above 35.4 MeV.

Our results were compared with the previously published data [6,8,13,16,21,26,27] and the theoretical prediction in the TENDL-2023 data library [17], shown in Fig. 10. Both our data and several earlier experimental results are higher than the theoretical

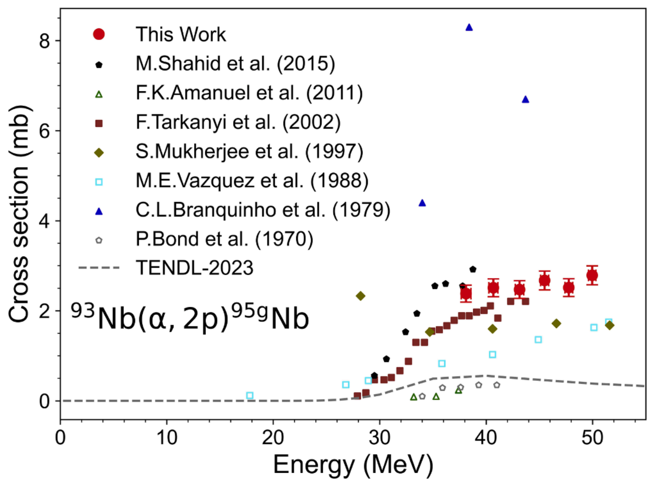

Fig. 10. Cross sections of the ^{93}Nb(α,2p)^{95g}Nb reaction, compared with the previously published data [6,8,13,16,21,26,27] and the theoretical values from the TENDL-2023 library [5].

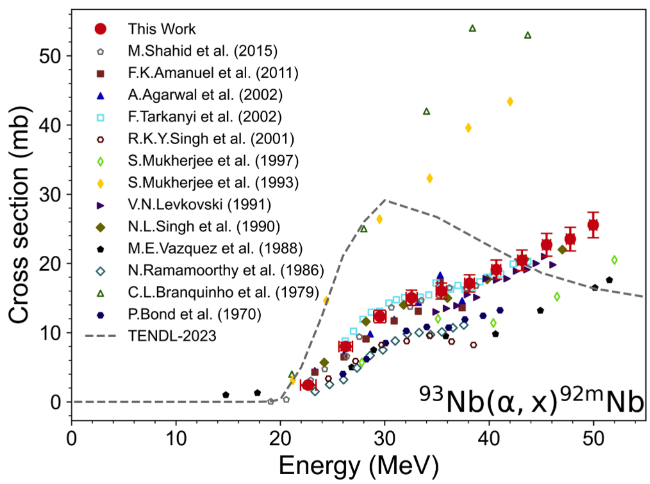

Fig. 11. Cross sections of the ^{93}Nb(α,x)^{92m}Nb reaction, compared with the previously published data [6,8,13–16,18–21,23,25,27] and the theoretical values from the TENDL-2023 library [5].

values.

3.7. Production cross sections of ^{92m}Nb

^{92g}Nb has an extremely long half-life ($T_{1/2}$ = 3.5 × 10^7 y), and cannot be detected by gamma-ray spectroscopy. In contrast, ^{92m}Nb ($T_{1/2}$ = 10.2 d) can be measured by counting the 934.4-keV gamma line after cooling time of 293.4–314.4 h.

Our results were compared with the previously published data [6,8,13–16,18–21,23,25,27] and the theoretical prediction in the TENDL-2023 library [17], shown in Fig. 11. Our results show good agreement with the recently published data [6,8,13,14,19,20] but exhibit a different trend compared to the theoretical values.

3.8. Production cross sections of ^{91m}Nb

^{91}Nb can be produced through both the ^{93}Nb(α,x)^{91}Nb reaction and electron capture and β^+ decay of ^{91g}Mo (ε+β^+: 100 %) and ^{91m}Mo (ε+β^+: 50 %, IT: 50 %). Since both ^{91}Mo states have short half-lives, 15.5 min for ^{91g}Mo and 64.6 s for ^{91m}Mo, contributions from indirect production via ^{91}Mo decay cannot be excluded in this analysis.

The cross sections of the long-lived ground state ^{91g}Nb ($T_{1/2}$ = 6.8 × 10^2 y) could not be determined. Only the cross sections of the metastable state ^{91m}Nb ($T_{1/2}$ = 60.86 d) were measured, using the gamma line at 1204.67 keV, after cooling time of 293.4–309.0 h.

Our results were compared with the previously published results [6,21] and the theoretical prediction in the TENDL-2023 data

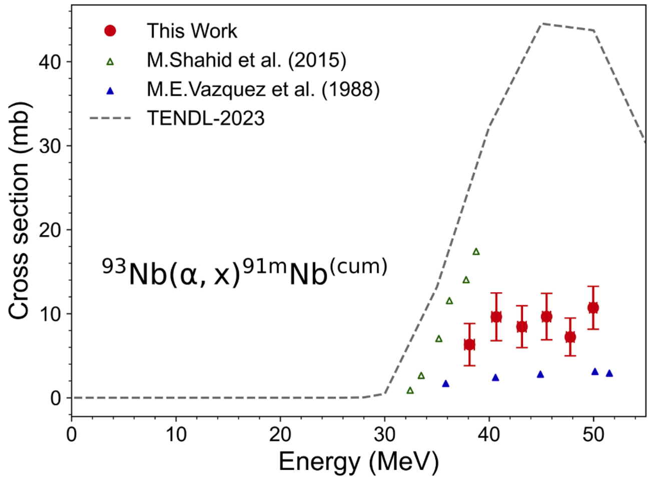

Fig. 12. Cumulative cross sections of the $^{93}Nb(\alpha,x)^{91m}Nb$ reaction, compared with the previously published data [6,21] and the theoretical values from the TENDL-2023 library [5].

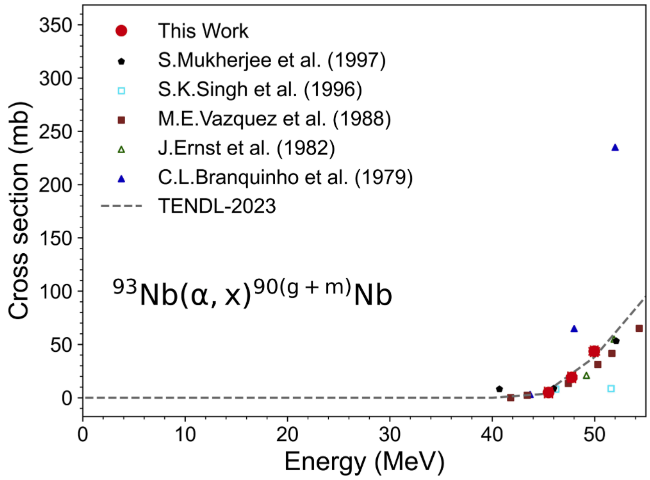

Fig. 13. Cross sections of the $^{93}Nb(\alpha,x)^{90(g+m)}Nb$ reaction, compared with the previously published data [16,17,21,24,25] and the theoretical values from the TENDL-2023 library [5].

library [17], shown in Fig. 12. The existing experimental results are scattered, and our results are lower than the prediction values.

3.9. *Production cross sections of* ^{90}Nb

^{90g}Nb can be produced through both the $^{93}Nb(\alpha,x)^{90g}Nb$ reaction and isomeric transition decay of ^{90m}Nb (IT: 100 %). Due to the extremely short half-life of ^{90m}Nb (18.91 s), it completely decayed before measurement. Therefore, the measured results represent the sum cross sections of $^{90(g+m)}Nb$. The cross sections were determined by counting the 1129.224-keV gamma-ray measured after cooling time of 34.6–36.7 h. Our results are compared with the published data [16,17,21,24,25] and the theoretical prediction in the TENDL-2023 library [5], shown in Fig. 13. Except for the data reported by Branquinho et al. [26] and Singh et al. [17], the existing experimental data show good agreement with the theoretical values from TENDL-2023.

3.10. *Production cross sections of* ^{89g}Zr

^{89g}Zr can be produced through both the $^{93}Nb(\alpha,x)^{89g}Zr$ reaction and the isomeric transition of ^{89m}Zr ($T_{1/2}$ = 4.2 min, IT: 93.77 %). A measurable signal for determining the cumulative cross section of ^{89g}Zr was only observed at 50.0 MeV, based on the analysis of the 909.2-keV gamma-ray ($I\gamma$ = 99.04 %) after a cooling time of 211.8 h. The contribution from the isomeric transition of ^{89m}Zr is considered negligible due to its very low production cross section predicted by TENDL-2023 at energies below 50 MeV (maximum: 0.004 mb) [5].

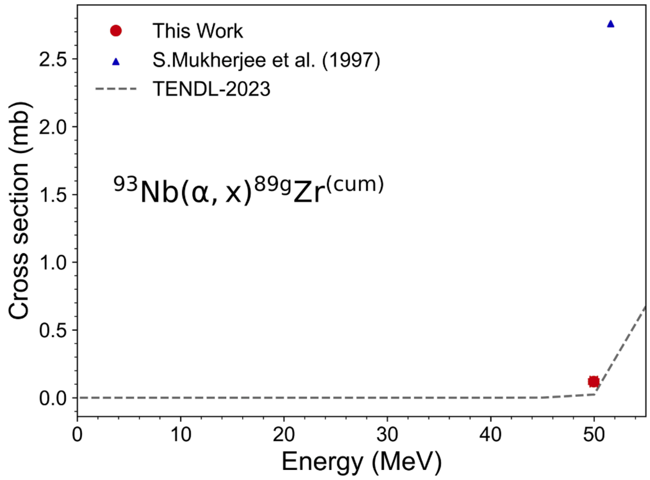

Fig. 14. Cumulative cross sections of the ^{93}Nb(α,x)^{89g}Zr reaction, compared with the previously published data [16] and the theoretical values from the TENDL-2023 library [5].

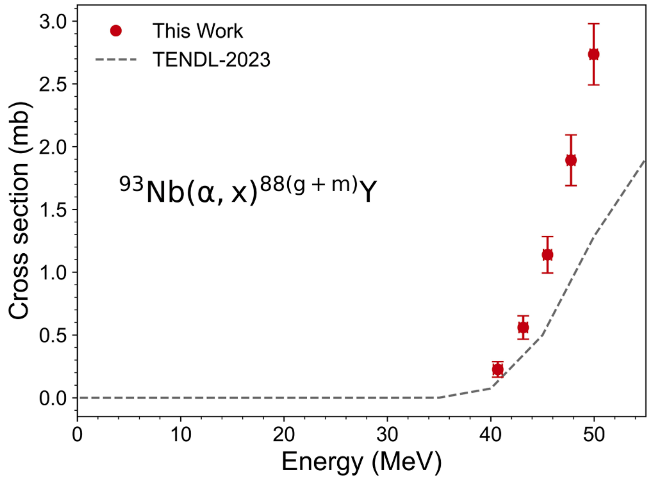

Fig. 15. Cross sections of the ^{93}Nb(α,x)$^{88(g+m)}$Y reaction, compared with the theoretical values from the TENDL-2023 library [5].

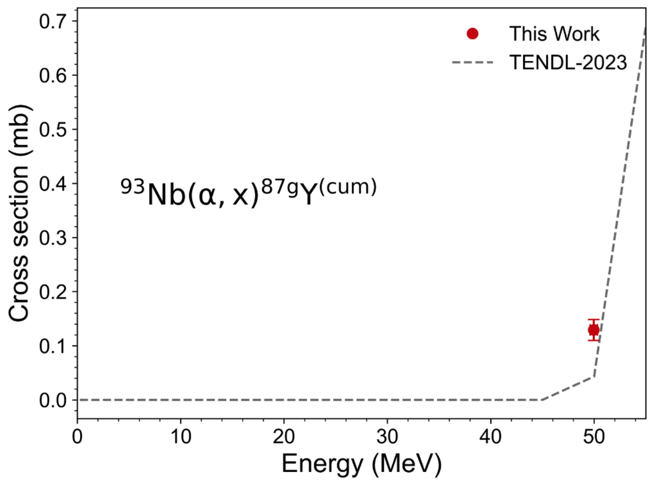

Fig. 16. Cumulative cross sections of the ^{93}Nb(α,x)^{87g}Y reaction, compared with the theoretical values from the TENDL-2023 library [5].

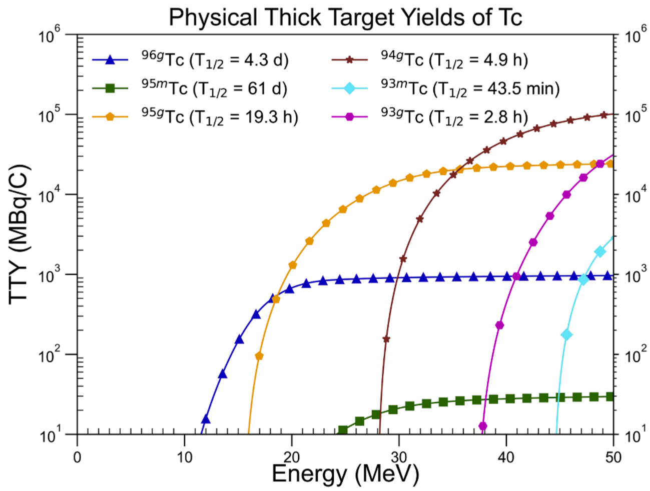

Fig. 17. The physical thick target yields of Tc radioisotopes, derived from interpolated cross section data obtained in this work.

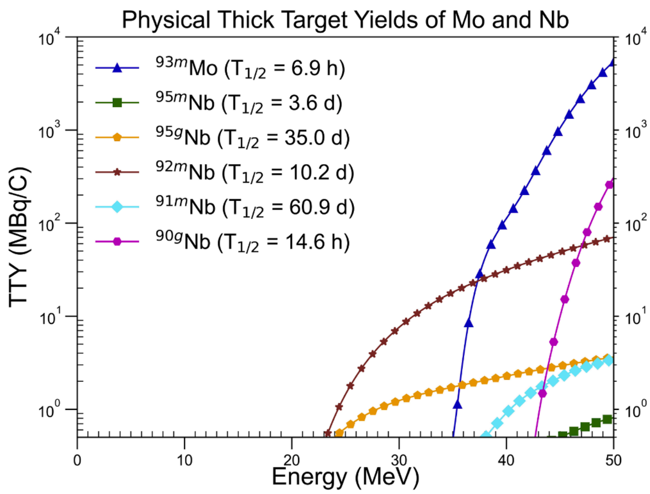

Fig. 18. The physical thick target yields of Mo and Nb radioisotopes, derived from interpolated cross section data obtained in this work.

Mukherjee et al. [16] provided one data point at 51.6 MeV, which is close to our experiment energy range and is thus compared with our result. Their value is much larger than ours. Our measurement agrees well with the TENDL-2023 prediction [5].

3.11. Production cross sections of ^{88}Y

^{88g}Y ($T_{1/2} = 106.6$ d) can be produced through both the $^{93}Nb(\alpha,x)^{88g}Y$ reaction and the decay of ^{88m}Y ($T_{1/2} < 1$ s) via 100 % isomeric transition. In this study, the $^{88(g+m)}Y$ cross sections were determined by detecting the 1836.1-keV gamma line measured after cooling time of 203.4–308.0 h.

No previous experimental data exist for ^{88}Y cross sections below 50 MeV. Compared with the TENDL-2023 theoretical predictions [5], our results show systematically higher values.

3.12. Production cross sections of ^{87g}Y

^{87g}Y ($T_{1/2} = 79.8$ h) can be produced through both the $^{93}Nb(\alpha,x)^{87g}Y$ reaction and the isomeric transition of ^{87m}Y ($T_{1/2} = 13.4$ h, IT: 98.43 %). The characteristic 380.8-keV gamma-ray from ^{87m}Y (Iγ: 78.05 %) was not observed even in early measurements, indicating the production of ^{87m}Y was small. A cumulative cross section of ^{87g}Y was determined using the 484.8-keV gamma-ray after a cooling time of 211.8 h, when the ^{87m}Y was totally decayed.

No experimental data for ^{87}Y cross sections below 50 MeV have been previously reported. Our results are consistent with the theoretical predictions from TENDL-2023 [5].

3.13. Physical thick target yields

Physical thick target yields [38] of $^{96g,95m,95g,94g,93m,93g}Tc$, ^{93m}Mo and $^{95m,95g,92m,91m,90g}Nb$ produced through alpha-particle-induced reactions on ^{93}Nb were estimated based on the interpolated cross sections measured in this work.

The physical thick target yields of Tc and other radioisotopes were shown in Fig. 17 and Fig. 18, respectively.

4. Conclusion

We measured the production cross sections of $^{96g,95m,95g,94g,93m,93g}Tc$, ^{93m}Mo, $^{95m,95g,92m,91m,90}Nb$, ^{89g}Zr and $^{88,87g}Y$ in the alpha-particle-induced nuclear reactions of ^{93}Nb. The experiment was performed at the RIKEN AVF cyclotron facility using the stacked-foil activation technique coupled with high-resolution gamma-ray spectrometry. The derived cross sections were compared with the previously reported experimental data [6–30] and the theoretical values of TALYS based TENDL-2023 library [5]. Based on interpolated experimental cross section values, we calculated the physical thick target yields for Tc, Nb and Mo radioisotopes. These results are expected to both optimize radionuclide production parameters and contribute to improvements in nuclear reaction modeling.

CRediT authorship contribution statement

He Huang: Writing – original draft, Methodology, Investigation. **Masayuki Aikawa:** Writing – review & editing, Supervision, Project administration, Methodology, Investigation, Funding acquisition. **Shuichiro Ebata:** Writing – review & editing, Methodology. **Kenta Sugihara:** Writing – review & editing, Methodology. **Zolbadral Tsoodol:** Writing – review & editing, Methodology. **Naoyuki Ukon:** Writing – review & editing, Methodology. **Hiromitsu Haba:** Writing – review & editing, Methodology. **Sándor Takács:** Writing – review & editing, Methodology. **Ferenc Ditrói:** Writing – review & editing, Methodology. **Zoltán Szűcs:** Writing – review & editing, Methodology. **Tamás Tornyi:** Writing – review & editing, Methodology.

Declaration of competing interest

The authors declare that they have no known competing financial interests or personal relationships that could have appeared to influence the work reported in this paper.

Acknowledgment

This work was carried out at RI Beam Factory operated by RIKEN Nishina Center and CNS, University of Tokyo, Japan. The authors would like to thank A. Nambu, Y. Shigekawa, Y. Kanayama, H. Shimizu, and S. Mitra of RIKEN Nishina Center for technical assistance with the experiment.

This work was supported by Japan Science and Technology Agency, Support for Pioneering Research Initiated by the Next Generation (JST SPRING), Grant Number JPMJSP2119.

This work was supported by Japan-Hungary Research Cooperative Program between JSPS and HUS, Grant number JPJSBP120193808 and NKM-43/2019.

This work was partly supported by Ministry of Innovation and Technology of Hungary from the National Research, Development and Innovation Fund, financed under the TKP2021 funding scheme, Project no. NKTA-42.

Reference

[1] T. Hayakawa, et al., ^{95g}Tc and ^{96g}Tc as alternatives to medical radioisotope ^{99m}Tc, Heliyon 4 (1) (2018) e00497, https://doi.org/10.1016/j.heliyon.2017.e00497.

[2] C. Winant, et al., Use of ^{94}Tc-MIBI PET data to model dynamic cardiac SPECT, J. Nucl. Med. 49 (1) (2008) 150, supplement, https://jnm.snmjournals.org/content/49/supplement_1/150P.4.

[3] H.M. Bigott, et al., Advances in the production, processing and microPET image quality of technetium-94m, Nucl. Med. Biol. 33 (7) (2006) 923–933, https://doi.org/10.1016/j.nucmedbio.2006.07.001.

[4] G. Katherine, et al., Radiotracers based on technetium-94m, Curr. Radiopharm. 4 (2) (2011) 90–101, https://doi.org/10.2174/1874471011104020090.

[5] A.J. Koning, et al., TENDL: complete nuclear data library for innovative nuclear science and technology, Nucl. Data Sheets 155 (2019) 1–55, https://doi.org/10.1016/j.nds.2019.01.002.

[6] M. Shahid, et al., Measurement of the excitation functions in alpha-induced reactions on ^{93}Nb from threshold energy to 39.5 MeV, J. Korean Phys. Soc. 67 (8) (2015) 1474–1481, https://doi.org/10.3938/jkps.67.1474.

[7] K. Kim, et al., Excitation function and isomeric ratio of Tc-isotopes from the $^{93}Nb(\alpha, xn)$ reaction, Nucl. Phys. A 935 (2015) 65–78, https://doi.org/10.1016/j.nuclphysa.2014.12.006.

[8] F.K. Amanuel, et al., Significant amount of pre-equilibrium contribution in the $\alpha+^{93}Nb$ system at energies ≈ 18-40 MeV, Chin. J. Phys. 49 (4) (2011) 884–892.

[9] C.S. Palshetkar, et al., Fusion of the weakly bound projectile ^{9}Be with ^{89}Y, Phys. Rev. C 82 (4) (2010) 044608. https://link.aps.org/doi/10.1103/PhysRevC.82.044608.

[10] M.Kumar Sharma, et al., A study of pre-equilibrium emission of neutrons in $^{93}Nb(\alpha, xn)$ reactions, Eur. Phys. J. A 31 (1) (2007) 43–51, https://doi.org/10.1140/epja/i2005-10318-5.

[11] B.P. Singh, et al., A study of pre-equilibrium emission in some proton- and alpha-induced reactions, Nucl. Instrum. Methods Phys. Res. A: Accel. Spectrom. Detect. Assoc. Equip. 562 (2) (2006) 717–720, https://doi.org/10.1016/j.nima.2006.02.030.

[12] S. Mukherjee, et al., Measurement and analysis of isomeric cross section ratios in the reaction $^{93}Nb(\alpha,2n)^{95}Tc$: Pre-equilibrium reaction mechanism, Phys. Rev. C 72 (1) (2005) 014609. https://link.aps.org/doi/10.1103/PhysRevC.72.014609.

[13] F. Tárkányi, et al., Measurement and evaluation of the excitation functions for alpha particle induced nuclear reactions on niobium, Nucl. Instrum. Methods Phys. Res. B: Beam Interact. Mater. At. 198 (1) (2002) 11–31, https://doi.org/10.1016/S0168-583X(02)01523-9.
[14] A. Agarwal, et al., Excitation function studies of α induced reactions for niobium and preequilibrium effects, Phys. Rev. C 65 (3) (2002) 034605, https://doi.org/10.1103/PhysRevC.65.034605.
[15] R. Singh, et al., Pre-equilibrium particle emission in α-induced excitation functions in niobium, Chin. J. Phys. 39 (4) (2001) 336–343.
[16] S. Mukherjee, et al., Analysis of the excitation functions from alpha particle induced reactions up to 120 MeV, Phys. Scr. 55 (4) (1997) 409, https://doi.org/10.1088/0031-8949/55/4/005.
[17] S. Singh, L. Chaturvedi, Alpha-particle induced excitation function studies up to 120 MeV, Indian J. Phys. A 70 (1) (1996) 155–160.
[18] S. Mukherjee, et al., Measurement and analysis of the excitation functions for alpha particle induced reactions on niobium, Pramana 41 (4) (1993) 329–338, https://doi.org/10.1007/BF02847397.
[19] V.N. Levkovskij, 1991, Activation cross section nuclides of average masses (A = 40–100) by protons and alpha-particles with average energies (E = 10–50 MeV), activation cross section by protons and alphas, USSR, Moscow (The data were taken from EXFOR database: https://www-nds.iaea.org/exfor).
[20] N.L. Singh, et al., Comparative study of pre-equilibrium models and mechanism of alpha particle induced reactions, J. Phys. Soc. Jpn. 59 (11) (1990) 3916–3924, https://doi.org/10.1143/JPSJ.59.3916.
[21] M.E. Vázquez, et al., (α, αxn) and (α, 2pxn) reactions on ^{93}Nb, J. Radioanal. Nucl. Chem. 121 (1) (1988) 203–219, https://doi.org/10.1007/BF02041462.
[22] J.R. Rao, et al., Non-equilibrium effects in alpha-particle-induced reactions in light, medium and heavy nuclei up to 120 MeV, J. Phys. G: Nucl. Phys. 13 (4) (1987) 535, https://doi.org/10.1088/0305-4616/13/4/017.
[23] N. Ramamoorthy, et al., Production of ^{96}Tc and ^{95m}Tc via the ^{93}Nb(α, xn) reactions, J. Radioanal. Nucl. Chem. 98 (1) (1986) 121–126, https://doi.org/10.1007/BF02060439.
[24] J. Ernst, et al., Investigation of α-induced reactions on niobium and tantalum, Z. Phys. Hadrons Nucl. 308 (4) (1982) 301–313, https://doi.org/10.1007/BF01415879.
[25] C.L. Branquinho, et al., Excitation functions and isomer ratios in the reactions ^{93}Nb(α, xn) (x = 1−4), J. Inorg. Nucl. Chem. 41 (5) (1979) 617–623, https://doi.org/10.1016/0022-1902(79)80343-7.
[26] C.L. Branquinho, et al., Spallation cross sections in the system ^{93}Nb + ^{4}He, J. Inorg. Nucl. Chem. 41 (6) (1979) 791–794, https://doi.org/10.1016/0022-1902(79)80267-5.
[27] P. Bond, S. Jha, Nuclear-structure and hyperfine-field studies with ^{95}Mo, Phys. Rev. C 2 (5) (1970) 1887–1897, https://doi.org/10.1103/PhysRevC.2.1887.
[28] T. Matsuo, et al., Cross-section ratios of isomeric nuclides produced in medium-energy (α, xn) reactions, Phys. Rev. 139 (4B) (1965) B886–B895. https://link.aps.org/doi/10.1103/PhysRev.139.B886.
[29] L.F. Hansen, M.L. Stelts, (α,n) reactions in some elements in the region of A =100, Phys. Rev. 136 (4B) (1964) B1000–B1005, https://doi.org/10.1103/PhysRev.136.B1000.
[30] J.M. Matuszek, T.T. Sugihara, The decay of 293 min Tc^{94}, Nucl. Phy. 42 (1963) 582–591, https://doi.org/10.1016/0029-5582(63)90758-2.
[31] T. Watanabe, et al., Beam energy and longitudinal beam profile measurement system at the RIBF, in: Proceedings of the International Particle Accelerator Conference (5th), 2014, pp. 3566–3568, https://doi.org/10.18429/JACoW-IPAC2014-THPME136.
[32] J.F. Ziegler, et al., SRIM – the stopping and range of ions in matter (2010), Nucl. Instrum. Methods Phys. Res. B: Beam Interact. Mater. At. 268 (11) (2010) 1818–1823, https://doi.org/10.1016/j.nimb.2010.02.091.
[33] Nuclear structure and decay data on-line library, Nudat 3.0. http://www.nndc.bnl.gov/nudat3/.
[34] NNDC Brookhaven national laboratory. https://www.nndc.bnl.gov/qcalc/.
[35] N. Otuka, et al., Isomer production studied with simultaneous decay curve analysis for alpha-particle induced reactions on natural platinum up to 29 MeV, Eur. Phys. J. A 60 (9) (2024) 195, https://doi.org/10.1140/epja/s10050-024-01383-7.
[36] F. Tárkányi, et al., Charged Particle Cross-Section Database for Medical Radioisotope Production: Diagnostic Radioisotopes and Monitor Reactions, International Atomic Energy Agency, 2001. https://www.iaea.org/publications/6050/charged-particle-cross-section-database-for-medical-radioisotope-production-diagnostic-radioisotopes-and-monitor-reactions.
[37] A. Hermanne, et al., Reference cross sections for charged-particle monitor reactions, Nucl. Data Sheets 148 (2018) 338–382, https://doi.org/10.1016/j.nds.2018.02.009.
[38] N. Otuka, S. Takács, Definitions of radioisotope thick target yields, Radiochim. Acta 103 (1) (2015) 1–6, https://doi.org/10.1515/ract-2013-2234.
[39] N. Otuka, et al., Towards a more complete and accurate experimental nuclear reaction data library (EXFOR): international collaboration between nuclear reaction data centres (NRDC), Nucl. Data Sheets 120 (2014) 272–276, https://doi.org/10.1016/j.nds.2014.07.065.